Kinetic Study of the Chlorination of Gallium Oxide

J.A. GONZÁLEZ, O.D. QUIROGA, and M. DEL C. RUIZ

The kinetics of the chlorination of gallium oxide in chlorine atmosphere was studied between 650 °C and 800 °C. The calculations of the Gibbs standard free energy variation with temperature for the reaction $Ga_2O_{3\,(S)} + 3Cl_{2\,(g)} \rightarrow 2GaCl_{3\,(g)} + 1.5O_{2\,(g)}$ show that direct chlorination is favorable above 850 °C. Thermogravimetric experiments were performed under isothermal and nonisothermal conditions. The effect of temperature, gas flow rate, and Cl_2 partial pressure were studied. The solids were characterized by X-ray diffraction (XRD) and scanning electronic microscopy (SEM). The nonisothermal results showed that chlorination of Ga_2O_3 starts at approximately 650 °C, with a mass loss of 50 pct at 850 °C. The isothermal results between 650 °C and 800 °C indicated that the reaction rate increased with temperature. The correlation of the experimental data with different solid-gas reaction models showed that the results are adequately represented by the model proposed by Shieh and Lee: $X = 1 - \{1 - b_{22}[b_{21}t + e^{-b_{21}t} - 1]\}^{1/(1-\gamma)}$. From this model, it was found that the rate of reaction for the chlorination of Ga_2O_3 is of the order 0.68 with respect to Cl_2 and the activation energy is 113.23 kJ/mol. On the other hand, the order of the activation rate of the interface surface is 0.111 with respect to Cl_2 and its activation energy is 23.81 kJ/mol.

I. INTRODUCTION

THE intensive use of metals in modern industry has led to the progressive exhaustion of primary metals, thus creating a need to use alternative sources such as industrial wastes, low grade minerals/ores, and polymetallic ores. Likewise, the exploitation of such sources requires the updating and development of processes that allow for maximum use of resources.

The advances in the development of materials with applications on a variety of fields ranging from medicine to space navigation has made it necessary to obtain high-purity metals. Although there exist a number of methods for the production of high-purity metals, liquid-liquid extraction from metallic halides in solution and the distillation of chlorides are the two most widely used techniques. In both cases, the obtainment of metallic halides constitutes the first stage in the process. One of the most widely used techniques for this stage is previous chlorination of materials such as metals, ores, metallic oxides, or industrial wastes.[1]

The use of chlorination in metal extractive procedures, by means of pyro- and hydrometallurgic methods, has attracted attention in recent decades and the use of chlorine chemistry may increase in the future. This is due to a number of factors, which include the high chlorination rates resulting from the elevated reactivity of Cl_2 and other chlorinating agents; the comparatively moderate temperature involved in the chlorination process; the low cost, variety, and availability of chlorinating agents; the favorable physical and chemical characteristics of certain metals; the properties of many chlorides (high solubility, wide variety of oxidation states, and ease of separation by liquid-liquid extraction or distillation); the selectivity of the treatment and separation processes; and the development of certain corrosion-resistant materials used for the manufacture of reactors.[2] On the other hand, the wastes from chlorination processes can be conveniently treated for the recovery of toxic materials, prior to their final disposal. The Cl_2 and chlorides in effluents can be easily dissolved in water or precipitated and subsequently recycled in the same unit, or they can be used for other purposes.

Gallium is present in nature in small amounts, usually associated with the ores of other common elements. It was discovered in the zinc ore blende in 1875. In 1896, it was found in bauxite, and it is also present in coal fly ashes. Gallium was initially obtained by electrodeposition on a mercury cathode, followed by cementation using sodium amalgam or by selective carbonization. This process has been currently discontinued due to environmental reasons. The current production of gallium comes mainly from the aluminum industry; however, in many alumina producing plants, much of the gallium originally present in bauxite and that not dissolved during aluminum extraction is discharged in the Bayer process residues, which constitute a potential source of gallium. In addition, since zinc ores also constitute a significant source of gallium and indium, both metals can be recovered from Zn leaching residues.[3,4,5]

Chaves *et al*.[5] studied the use of resins in the recovery of Ga as a byproduct of the Brazilian Zn and Al industries. Nishihama *et al*. investigated the recovery of Ga and In from zinc refinery residues, by liquid-liquid extraction using D2EHPA, obtaining 98.9 and 87.9 pct efficiency for In and Ga, respectively.[6] Nakayama and Egawa investigated the recovery of Ga from Bayer solutions containing large amounts of Al, using Kelex-100-loaded ion-exchange resin.[7] The production of high-purity Ga, In, and Cd for electronic applications has been studied by Ohwa *et al*., using a chloride refining process.[8]

J.A. GONZÁLEZ, Associate Researcher, and M. DEL C. RUIZ, Associate Professor and Senior Researcher; are with the Institute of Investigations in Chemical Technology (INTEQUI), Universidad Nacional de San Luis and Consejo Nacional de Investigaciones Científicas y Técnicas, 5700 San Luis, Argentina. Contact e-mail: mruiz@unsl.edu.ar O.D. QUIROGA, Professor and Senior Researcher, is with the Institute of Investigations for Chemical Industry (INIQUI), Universidad Nacional de Salta and Consejo Nacional de Investigaciones Científicas y Técnicas, 4400 Salta, Argentina.

Manuscript submitted July 15, 2003.

Gallium is a material of vital importance for the manufacturing of semiconductors, and, in the future, efficient recycling processes will be needed for the recovery of these metals. It is particularly important to pursue research that permits recovery of Ga and In from electronic devices containing compounds such as GaAs, InGaAs, and InP, among others. The use of chlorination for the recovery of these metals is currently under investigation in Europe, Japan, and the United States,[9] due to the above-mentioned advantages of this technology as compared to other metal recovery methods.

In this work, we studied the chlorination of pure gallium oxide in chlorine atmosphere, in order to know the effect of different variables upon the system reactivity and to propose a mechanism and a kinetic reaction model that explains the experimental data and contributes to the understanding of the chlorination of gallium containing materials.

II. THERMODYNAMIC CONSIDERATIONS

The global reaction involved in this process is

$$Ga_2O_3\,(S) + 3Cl_2\,(G) \rightarrow 2GaCl_3\,(G) + 1.5O_2\,(G) \quad [1]$$

The reactants are a solid and a gas, and the obtained products are all fluids, since $GaCl_3$ is a gas above 270 °C. The thermodynamic calculations were performed using HSC chemistry for Windows.[10] The variation of Gibbs standard free energy (kJ/mol Ga_2O_3) for Reaction [1] as a function of temperature (deg Celsius) occurs according to

$$\Delta G^\circ = 168.584 - 19.39*10^{-2}T \quad [2]$$

From Eq. [2], ΔG° is positive at low temperatures, and takes negative values at temperatures above 870 °C.

Figure 1 shows the phase stability diagram for the Ga-O-Cl system at 680 °C and 780 °C. The values for the partial pressures of species $GaCl_3$ (g) and O_2 (g) calculated in pure Cl_2 atmosphere were 0.310 and 0.232 atm at 680 °C and 0.645 and 0.489 atm at 780 °C, respectively. These calculations and phase stability diagrams were obtained using the data in Reference 10. According to these diagrams, gallium oxide can react with chlorine at those temperatures, and, under the conditions of this study, the only chlorination product is $GaCl_3$.

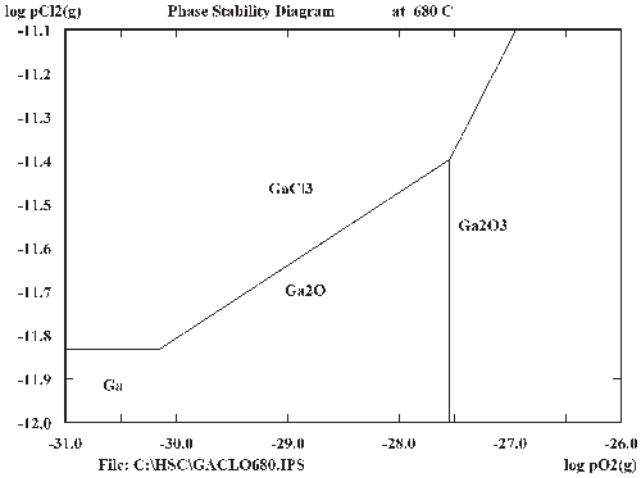

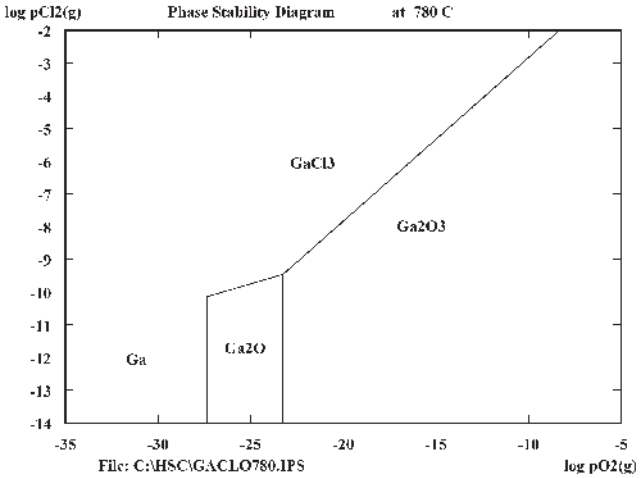

Fig. 1—Diagram of phase stability for the Ga-O-Cl system at 680 °C and 780 °C.

III. EXPERIMENTAL

A. *Materials*

The chlorination experiments were performed using Ga_2O_3, Fluka AG, 99.99 pct purity. The results of scanning electron microscopy (SEM) analysis are shown in Figures 2(a) through (c). As seen in Figure 2(a) the particle sizes are between 1 and 200 μm and exhibit varied morphology including very small lentil-shaped particles forming larges conglomerates, and elongated particles approximately 200-μm long. Figure 2(b) shows a conglomerate of small particles, and the flat surface of some larger particles. Figure 2(c) shows the surface of a conglomerate of small particles.

Figure 3 shows the diffractogram of Ga_2O_3, and it can be seen that the solid is crystalline and matches the JCPDS 41-1103 file,[11] which corresponds to a monocyclic structure *C*2/*m*.

The gases used were 99.9 pct pure chlorine (Indupa, Argentina) and 99.9 pct pure nitrogen (A.G.A., Argentina).

B. *Experimental Equipment and Procedure*

The equipment used for the chlorination assays is shown in Figure 4. Isothermal and nonisothermal experiments were performed, studying the effect of temperature, the reaction time, and the chlorine flow and partial pressure.

Since the chlorination products are volatile in the studied temperature range, the course of the reaction was followed measuring the mass changes of the sample in each experimental assay. To do this, the masses of the sample and sample holder were previously determined and the mass of the residue was determined after each experiment so as to know the mass changes as a function of each studied variable.

For the isothermal assays, a sample of known mass, approximately 70 mg, was supported on a quartz crucible and placed into the reaction zone, under N_2 flow, until reaching the working temperature. The temperature of the reaction was obtained placing the thermocouple on the solid sample bed. Once the conditions selected for the experiment had been set, the three-way valves were turned so

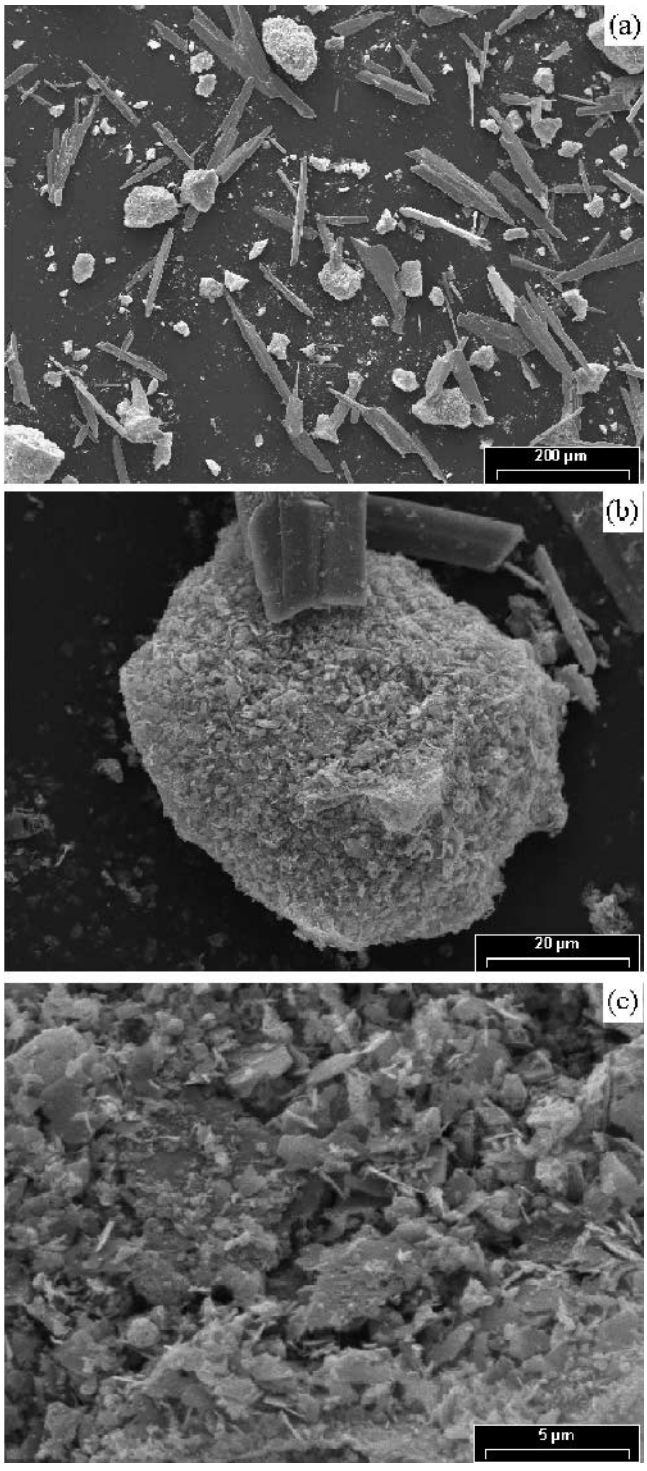

Fig. 2—Morphology of the Ga_2O_3 particles: (*a*) overall view, (*b*) morphology of particles of different sizes, and (*c*) superficial appearance of a conglomerate.

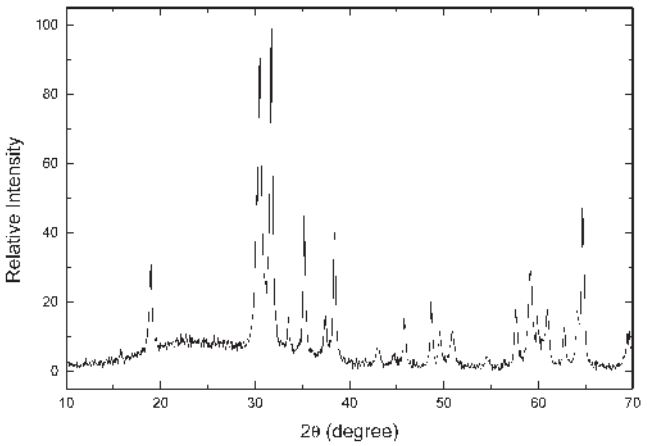

Fig. 3—X-ray diffractogram of Ga_2O_3.

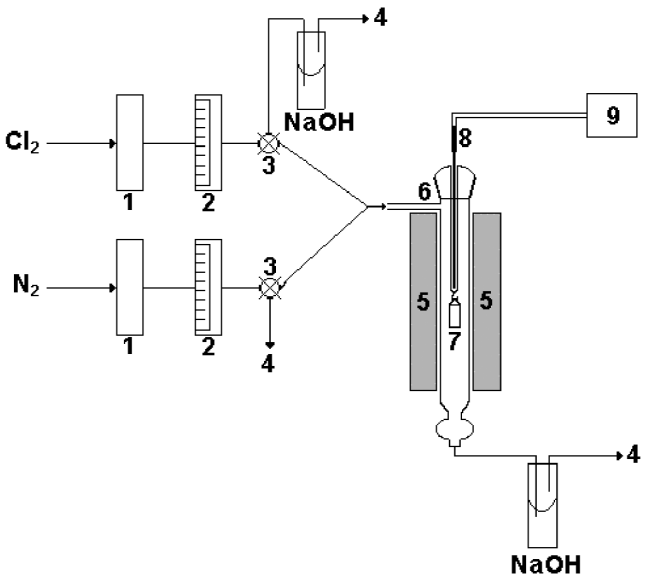

Fig. 4—Diagram of the experimental equipment: (1) drying units, (2) flowmeters, (3) three-way valves, (4) venting, (5) furnace, (6) quartz reactor, (7) quartz crucible, (8) thermocouple, and (9) temperature control unit.

that N_2 was sent to venting and pure Cl_2 or the Cl_2-N_2 mixture was let into the reactor. At that point, the starting time was recorded. After the reaction time, the reactor was purged with N_2 current. The total flow of gas was always 100 mL/min. The residue remaining in the crucible was cooled and weighed in order to determine sample mass changes.

For the nonisothermal experiments, sample chlorination was performed at a set temperature and for a fixed time of 10 minutes. Once the assay had finished, the reactor was purged with N_2 and the sample was weighed. Subsequently, chlorination was repeated at a higher temperature. The same flow and mass conditions as in isothermal experiments were used. The temperature increase between each point was 50 °C.

The mass loss suffered by the sample during nonisothermal experiments was expressed as mass loss percent, Δm pct, according to the following equation:

$$\Delta m \text{ pct} = \frac{m_f - m^\circ}{m^\circ} * 100 \qquad [3]$$

The results of isothermal experiments were expressed as fraction of conversion of the solid reagent, defined as

$$X = \frac{m^\circ - m_f}{m^\circ} \qquad [4]$$

where m° and m_f stand for the initial and final masses of Ga_2O_3, respectively.

IV. RESULTS AND DISCUSSION

A. *Nonisothermal Chlorination*

The experimental results of nonisothermal chlorination are shown in Figure 5. As can be observed from this figure, the mass loss of Ga_2O_3 in Cl_2 by direct chlorination starts at about 650 °C, reaching 50 pct mass loss at 850 °C. The mass loss in N_2 atmosphere is negligible in the analyzed temperature range.

B. *Effect of Temperature and Reaction Time*

The effect of temperature and reaction time on the chlorination of Ga_2O_3 was studied in the intervals between 680 °C and 800 °C and 2.5 and 150 minutes, respectively. The upper and lower limits were selected considering the results of nonisothermal chlorination, so that the mass changes of the samples during the reaction could be appreciated.

The results of isothermal chlorination (Figure 6) show that the reaction rate increases with temperature, and also that the conversion of Ga_2O_3 is practically total at 800 °C and 90 minutes reaction time.

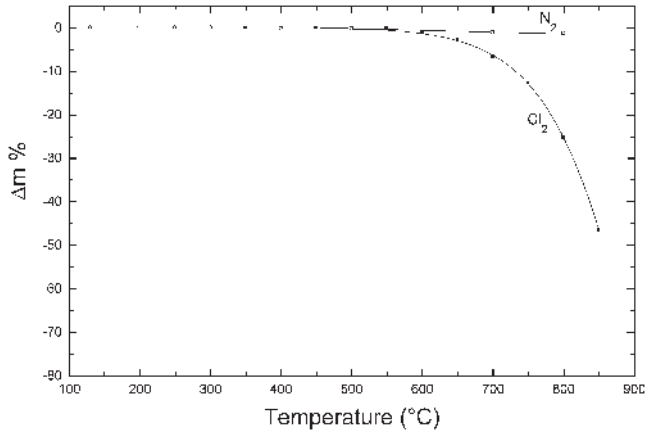

Fig. 5—Nonisothermal chlorination of Ga_2O_3 in N_2 and Cl_2 atmospheres.

C. *Effect of Chlorine Flow and Partial Pressure*

The study of the effect of the chorine flow rate was performed in an interval between 40 and 170 mL/min. There were no appreciable changes in Ga_2O_3 conversion in the studied range. The effect of the feed composition on the chlorination of Ga_2O_3 was studied at 780 °C, using N_2 as a diluent and a total flow of 100 mL/min. Cl_2 partial pressures of 0.3, 0.5, 0.8, and 1 atmosphere were investigated. As shown in Figure 7, the experimental results indicate an appreciable variation of the system reactivity with Cl_2 partial pressure.

D. *Characterization of the Reaction Residues*

The results of SEM analysis of the residues of Ga_2O_3 chlorination are shown in Figures 8(a) through (c). Comparison of Figures 8(a) and 2(a) shows that most of the smaller particles were consumed. At the same time, both the small particle conglomerates and the elongated particles occurred by a uniform attack on their surface, as can be clearly observed comparing Figures 2(b) and (c) with 8(b) and (c), respectively. From both figures, it can also be noted that there was no sintering or morphological changes in the larger Ga_2O_3 crystals.

The X-ray diffraction (XRD) analysis of the chlorination residues obtained under different experimental conditions did not show changes in the crystalline structure of Ga_2O_3. Likewise, no chlorinated compounds were detected in the residue by XRD.

E. *Kinetic Models*

Bamford and Tipper[12] state that the kinetic treatment of noncatalytic solid-gas heterogeneous reactions can be performed by comparing series of measurements of X (conversion) – t (time) with models that are formulated taking into account the initial state and the evolution experienced by the different dependent or independent variables involved in the process. When the reaction is simple, such as

$$aA_{(G)} + bB_{(S)} \rightarrow qQ_{(G)} \qquad [5]$$

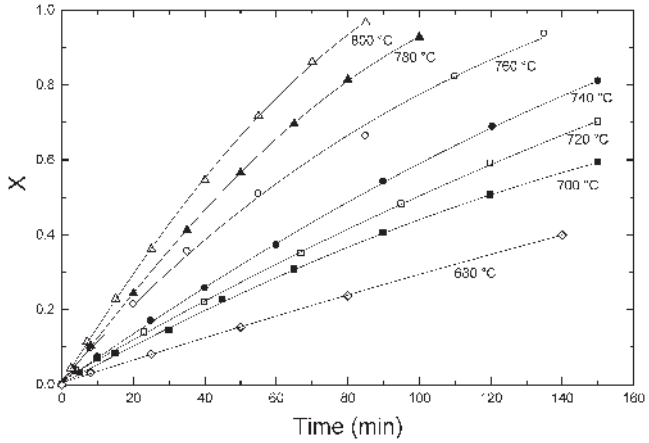

Fig. 6—Chlorination of Ga_2O_3 at different temperatures.

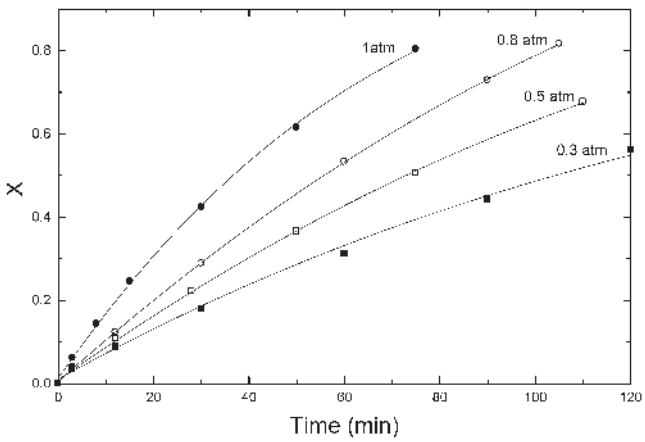

Fig. 7—Effect of Cl_2 partial pressure on the chlorination of Ga_2O_3.

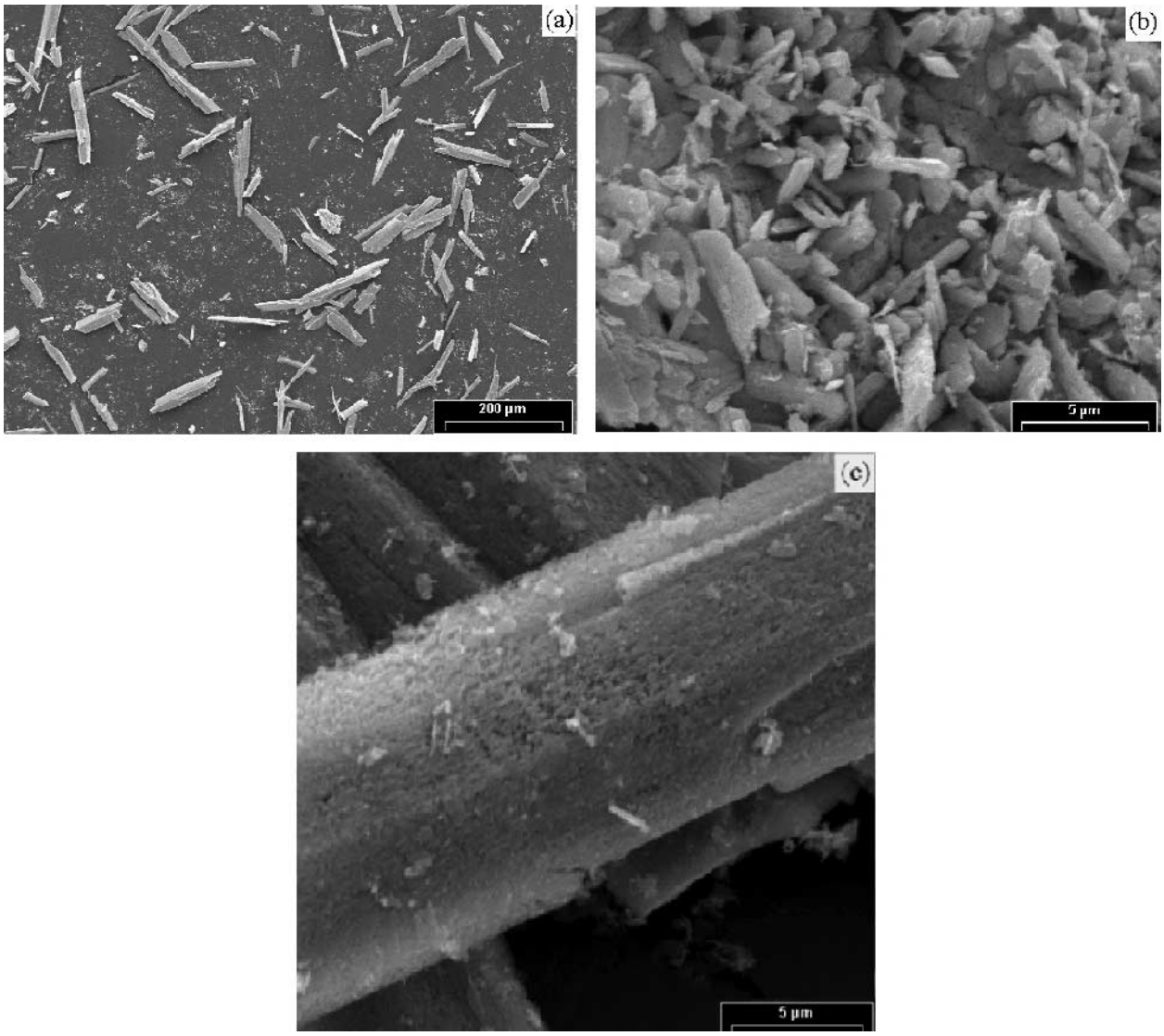

Fig. 8—SEM analysis of the chlorination residue: (*a*) overall view of a chlorinated residue, (*b*) surface of the conglomerate after the chlorination, (*c*) attacked elongated particle.

and the solid reagent is pure and nonporous, the development of kinetic models is based on the following equation:

$$\frac{dX}{dt} = \frac{bM_B r_s \Omega_r}{m^0} \quad [6]$$

where X, M_B, and m^0 are the conversion, the molecular weight, and the initial mass of the solid reagent, respectively; Ω_r is the reaction interface; and r_s is the reaction rate per unit of reaction interface.

In Eq. [6], r_s is a function of the temperature, T, and of the partial pressure of the fluid chemical species, commonly expressed by models of the Langmuir – Hinshelwood – Hougen – Watson type, as in the following example:

$$r_S = \frac{k(p_{As} - p_{Qs}/K)}{1 + k_1 p_{As} + k_2 p_{Qs}} \quad [7]$$

or else by models of the potency-law type:

$$r_S = k p_{As}^n \quad [8]$$

where p_{As} and p_{Qs} are the partial pressures of the fluid reagent and product A and Q, respectively, evaluated on the reaction interface.

In Eq. [6], Ω_r is a function of the extension of the interface area and the solid reactivity. The extension depends on geometrical factors and on the accessibility of the fluid reagent. As can be seen in Bamford and Tipper[12] and in Quiroga *et al.*,[13] if the particle is nonporous or there is no formation of solid products on it, the modeling of Ω_r is carried out as a function of the type of reactivity exhibited by the solid reagent sample. It has been experimentally observed that solids can exhibit three types of reactivity.

1. *Type A*

Local and temporally uniform reactivity: this type occurs when the interface surface exhibits a uniformly reactive behavior that does not depend on the time or on the particle internal coordinates. If the reacting particle is made up of a nonporous pure solid reagent ($\varepsilon^\circ = 0$), then $\Omega_r = \Omega$,

which depends not only on the particle shape and size, can be expressed as a function of X by the following equation:

$$\Omega = \Omega^0(1 - X)^{\gamma} \quad [9]$$

where Ω^0 is the initial external surface area of the particle; γ is a shape coefficient of the particle ($\gamma = 2/3$, if the particle is spherical; $\gamma = 1/2$, if it is an elongated, needle-shaped particle; and $\gamma = 0$, if it is disc shaped or a flat plate).

If the reaction occurs at constant c_{As} and T, then, by combining Eqs. [6], [8], and [9] and integrating the resulting equation, the following correlation equation is obtained:

$$\text{Model 1:} \quad X = 1 - (1 - b_{11}t)^{1/(1-\gamma)} \quad [10]$$

with b_{11} defined as

$$b_{11} = \frac{b(1 - \gamma)M_B\, k p_A^n \Omega^{\circ} t}{m^{\circ}} \quad [11]$$

Model 1 is used for correlating kinetic data obtained from noncatalytic solid-fluid reactions that satisfy the following conditions: (1) the reaction is carried out at constant c_{As} and T; (2) there is no formation of solid products that remain adhered to the particles; and (3) the solid sample is formed by particles of nonporous pure solid reagent with a constant reactivity.

2. *Type B*

Topochemical or autolocalized reactivity—this type can occur when the formation of Ω_r—takes place in preferential sites of the particle interface surface. As can been seen in Bamford and Tipper,[12] Quiroga *et al.*,[13] and Delmon,[14] the modeling of Ω_r is based on the theory of nucleation and growth developed by Avrami. From this theory, a number of models can be developed that differ in regard to the nucleation type, the mechanisms involved in the nucleation rate, and the shape of the nuclei.

3. *Type C*

Locally uniform and initially variable reactivity—this type occurs when the initial reactivity of the interface surface is null and gradually grows as the contact time between the reagents increases. Shieh and Lee[15] have established that the variation experienced by the solid reactivity at the start of the reaction is due to physicochemical phenomena that occur on the interface surface of the solid reagent. According to these authors, the formation rate of Ω_r can be expressed as follows:

$$\frac{d\theta}{dt} = (1 - \theta)r_{\Omega} \quad [12]$$

where $\theta = \Omega_r/\Omega$; r_{Ω} is the formation rate of Ω_r.

The formulation of r_{Ω} is done as a function of the rate of the rate-controlling stage of the physicochemical phenomenon that takes place in Ω. For example, if the reaction initial rate is controlled by the rate of the adsorption-reaction-desorption stages, a good approximation of r_{Ω} is obtained by the following expression:

$$r_{\Omega} = k_{\Omega}\, p_A^m \quad [13]$$

Combining and integrating Eqs. [12] and [13], and taking into account that when the solid reagent is pure and nonporous, $\Omega = \Omega^{\circ}(1 - X)^{\gamma}$, Eq. [14] is obtained:

$$\Omega_r = \Omega^{\circ}(1 - X)^{\gamma}[1 - e^{-k_{\Omega}\, p_A{}^m t}] \quad [14]$$

Note that for $t \to \infty$, Eq. [14] is reduced to Eq. [9].

Finally, if the reaction is carried out at constant c_{As} and T, by combining and integrating Eqs. [6], [8], and [14], the following correlation equation is obtained:

$$\text{Model 2:} \quad X = 1 - \{1 - b_{22}[b_{21}t + e^{-b_{21}t} - 1]\}^{1/(1-\gamma)} \quad [15]$$

with b_{21} and b_{22} defined as

$$b_{21} = k_{\Omega}\, p_A^m \qquad b_{22} = \frac{b(1 - \gamma)M_B\, k p_A^n \Omega^{\circ}}{m^{\circ} k_{\Omega}\, p_A^m} \quad [16]$$

Model 2 is used for correlating kinetic data obtained from noncatalytic solid-fluid reactions that satisfy the following conditions: (1) the reaction is carried out at constant c_{As} and T; (2) there is no formation of solid products that remain adhered to the particles; (3) the solid sample is formed by particles of nonporous pure solid reagent with variable initial reactivity. It is noted that for $t \to \infty$, the Eq. [15] is reduced to Eq. [10].

F. *Results of the Kinetic Treatment*

The experimental data of the chlorination of Ga_2O_3

$$Ga_2O_{3(S)} + 3Cl_{2(G)} \to 2\, GaCl_{3(G)} + 1.5\, O_{2(G)}$$

were treated by a software that includes models 1 and 2 and a large set of models developed on the basis of the nucleation and growth theory. This treatment showed that models 1 and 2 with $\gamma = 2/3$ present the lowest associated regression error. Table I presents the estimates of the parameters (columns b_{11}, b_{21}, and b_{22}) and the associated regression errors (columns $\bar{\varepsilon}_{r1}$ and $\bar{\varepsilon}_{r2}$) of each model for each run. Comparing the estimates of columns $\bar{\varepsilon}_{r1}$ and $\bar{\varepsilon}_{r2}$ one by one, it is observed that the associated regression errors of model 2 are lower than those of model 1. It is also observed that the associated errors of model 1 increase with increasing T and decreasing P_{Cl_2}, while the associated errors of model 2 do not exhibit any systematic tendency. Considering these observations and the fact that the kinetic mechanism involved in model 2 fits better with noncatalytic solid-gas heterogeneous reactions, as well as the fact that its adjunct regression errors at each level are lower than 1 pct, it is possible to consider model 2 more probable than model 1.

Finally, using the data from Table I for model 2 and by means of the mathematical treatment of the kinetic coefficients b_{21} *and* b_{22}, the following expressions are obtained for r_s and r_{Ω}:

$$r_s = 5.7610^3\, e^{-113.23/RT}\, p_{As}^{0.68} \qquad r_{\Omega} = 11.33\, e^{-23.810/RT}\, p_{As}^{0.111}$$

The results of the correlation of experimental data by model 2 are shown in Figure 9.

V. CONCLUSIONS

The chlorination of Ga_2O_3 with Cl_2 gas is appreciable at temperatures above 650 °C, and the conversion of Ga_2O_3 is practically total at 800 °C for a reaction time of 90 minutes.

The extension of Ga_2O_3 chlorination in Cl_2 atmosphere increases with temperature and Cl_2 partial pressure.

The experimental data were correlated with different kinetic models, finding that model 2, $X = 1 - \{1 - b_{22}[b_{21}t + e^{-b_{21}t} - 1]\}^{1/(1-\gamma)}$, is the one that best represents the results of Ga_2O_3 chlorination. Model 2 fits better with the kinetic mechanism

Table I. Results of the Kinetic Treatment of the Experimental Data of Ga_2O_3 Chlorination

			Model 1 $X = 1 - (1 - b_{11}t)^3$		Model 2 $X = 1 - \{1 - b_{22}[b_{21}t + e^{-b_{21}t} - 1]\}^3$		
Run	T (°C)	P_{Cl_2} (atm)	$\bar{\varepsilon}_{r1}$ (Pct)	$b_{11} \cdot 10^3$	$\bar{\varepsilon}_{r2}$ (Pct)	b_{21}	$b_{22} \cdot 10^3$
1	680	1	0.69	1.13	0.49	0.629	1.97
2	700	1	0.58	1.77	0.67	0.574	3.11
3	720	1	1.29	2.13	0.80	0.586	5.35
4	740	1	1.28	3.70	0.87	0.640	7.68
5	760	1	0.80	5.37	0.70	0.650	7.07
6	780	1	1.40	6.76	0.60	0.815	9.16
7	800	1	2.67	8.28	0.78	0.819	12.80
8	780	0.8	0.83	5.28	0.66	0.838	6.29
9	780	0.5	1.34	2.94	0.81	0.766	3.84
10	780	0.3	3.12	2.21	0.95	0.728	2.86

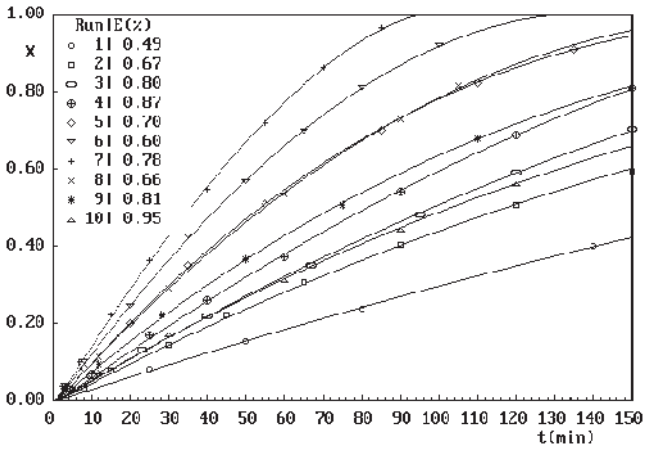

Fig. 9—Correlation of the experimental data of Ga_2O_3 chlorination with the experimental model $X = 1 - \{1 - b_{22}[b_{21}t + e^{-b_{21}t} - 1]\}^{1/(1-\gamma)}$.

of the stages involved in noncatalytic gas-solid heterogeneous reactions. Furthermore, it permitted establishment of the fact that the formation of the reaction interface is not instantaneous, and revealed that at the start of the reaction, the rate is controlled by the desorption rate of the fluid product.

ACKNOWLEDGMENTS

This work was supported by Universidad Nacional de San Luis and Consejo Nacional de Investigaciones Científicas y Técnicas, Argentina. The authors appreciate the useful suggestions of Doctor J.B. Rivarola.

NOMENCLATURE

a,b,q	stoichiometric coefficients of the gaseous reagent, solid reagent, and gaseous product, respectively
$A_{(G)}$, $B_{(S)}$, $Q_{(S)}$	gaseous reagent, solid reagent, and gaseous product, respectively
b_{11}, b_{21}, b_{22}	coefficients defined by Eqs. [11] and [16], respectively
C_{As}	molar concentration of the gaseous reagent, evaluated on the reaction interface
k	kinetic constant of fluid-solid reaction
k_1	kinetic constant of gaseous reagent adsorption
k_2	kinetic constant of gaseous product desorption
k_Ω	kinetic constant of reaction interface formation
K	equilibrium constant
M_B	molecular weight of the solid reagent
m_f	final Ga_2O_3 mass
m^0	initial Ga_2O_3 mass
m	order of reaction with respect to the formation of the reaction interface
n	order of reaction with respect to the fluid reagent
p_A	partial pressures of gaseous reagent and gaseous product
p_{As}, p_{Qs}	partial pressures, evaluated on the reaction interface, of gaseous reagent and gaseous product, respectively
p_{Cl_2}	partial pressure of gaseous reagent Cl_2
r_S	solid-fluid reaction rate per unit of reaction interface
r_Ω	formation rate of reaction interface
T	temperature
t	time
X	fraction of conversion of the solid reagent

Greek letters

Δm pct	mass loss percentage, defined by Eq. [3]
ε	particle porosity
ε^0	initial particle porosity
$\bar{\varepsilon}_{r1}$ (pct)	regression error associated with model 1
$\bar{\varepsilon}_{r2}$ (pct)	regression error associated with model 2
γ	particle shape factor
Ω	particle external surface
Ω^0	external surface of the initial particle
Ω_r	reaction interface
θ	relation between reaction interface and particle surface

REFERENCES

1. J.E. Hoffmann: *JOM*, 1991, vol. 43, pp. 18-23.
2. P.K. Jena and E.A. Brocchi: *Mineral Processing Extr. Metall. Rev.*, 1997, vol. 16 pp. 211-37.
3. D.A. Kramer: *Bureau of Mines, Information Circular*, 1988, vol. 9208, pp. 1-25.
4. E.Y.L. Sun: *JOM Rev. Extr. Metall.*, 1991, vol. 43, pp. 53-61.

5. A. Pinto Chaves, A. Abräo, and W. Avritscher: *Global Symp. on Recycling, Waste Treatment and Clean Technology*, I. Gaballah, J. Hager, and R. Solozabal, eds., TMS and INHSMET, Spain, 1999, pp. 1363-71.
6. S. Nishihama, T. Hirai, and I. Komasawa: *Ind. Eng. Chem. Res*., 1999, vol. 38, pp. 1032-39.
7. M. Nakayama and H. Egawa: *Eng. Chem. Res*., 1997, vol. 36, pp. 4365-68.
8. H. Ohwa, M. Yukinobu, J. Nabeshima, and M. Yasukawa: *Extr. Metall*., 89, 1989, pp. 885-98.
9. S. Kubo, M. Yukinobu, O. Yamamoto, G. Nabeshima, and J. Okajima: *2nd Int. Symp.—Recycling of Metals and Engineered Materials*, J.H.L. Van Linden, D.L. Stward, Jr., and Y. Sahai, eds., TMS, Warrendale, PA, 1990, pp. 505-13.
10. *HSC Chemistry for Windows version 5.1*, Outokumpu Research, Pori, Finland, 2003.
11. Card of JCPDS, *Powder Difraction Files*, International Centre for Diffraction Data, PA. 1993.
12. C.H. Bamford and C.F.H. Tipper: *Comprehensive Chemical Kinetics*, Elsevier Scientific Publishing, 1980, vol. 22,
13. O.D. Quiroga, J.R. Avanza, and A.J. Fusco: *Modelado Cinético de las Transformaciones Fluido-Sólido Reactivo*, Editorial Universitaria de la Universidad del Nordeste (EUDENE), Santuis, Argentina, 1996, pp. 148-60.
14. B. Delmon: *Introduction a la Cinétique Hétérogéne*, Editions Technip, Paris, 1969.
15. M.D. Shieh and C. Lee: *Chem. Eng. Sci*., 1992, vol. 47, pp. 4017-25.